nature climate change

Analysis

https://doi.org/10.1038/s41558-024-02180-2

Projections of multiple climate-related coastal hazards for the US Southeast Atlantic

Received: 4 May 2024

Accepted: 10 October 2024

Published online: 21 November 2024

Check for updates

Patrick L. Barnard[1] ✉, Kevin M. Befus[2], Jeffrey J. Danielson[3], Anita C. Engelstad[1], Li H. Erikson[1], Amy C. Foxgrover[1], Maya K. Hayden[1], Daniel J. Hoover[1], Tim W. B. Leijnse[4], Chris Massey[5], Robert McCall[6], Norberto C. Nadal-Caraballo[5], Kees Nederhoff[6], Andrea C. O'Neill[1], Kai A. Parker[1], Manoochehr Shirzaei[7], Leonard O. Ohenhen[7], Peter W. Swarzenski[1], Jennifer A. Thomas[1], Maarten van Ormondt[6], Sean Vitousek[1], Kilian Vos[8], Nathan J. Wood[9], Jeanne M. Jones[9] & Jamie L. Jones[9]

Faced with accelerating sea level rise and changing ocean storm conditions, coastal communities require comprehensive assessments of climate-driven hazard impacts to inform adaptation measures. Previous studies have focused on flooding but rarely on other climate-related coastal hazards, such as subsidence, beach erosion and groundwater. Here, we project societal exposure to multiple hazards along the Southeast Atlantic coast of the United States. Assuming 1 m of sea level rise, more than 70% of the coastal residents and US$1 trillion in property are in areas projected to experience shallow and emerging groundwater, 15 times higher than daily flooding. Storms increase flooding exposure by an order of magnitude over daily flooding, which could impact up to ~50% of all coastal residents and US$770 billion in property value. The loss of up to ~80% of present-day beaches and high subsidence rates that currently affect over 1 million residents will exacerbate flooding and groundwater hazard risks.

With more than 1 billion people estimated to be living in the global coastal zone (that is, elevation <10 m) by mid-century[1], including over 300 million living below annual flooding levels[2], sea level rise (SLR)-driven coastal hazards through the twenty-first century may displace human populations in low-lying areas, leading to major global security challenges[3]. Coastal flood risk will increase exponentially throughout the twenty-first century even under moderate SLR trajectories[4], affecting ecosystems, cultural and natural resources, and community development and well-being[5]. In developing adaptation strategies to support resilient and sustainable communities, solutions must consider a suite of connected hazards that could exacerbate coastal risk as SLR continues to accelerate, including flooding[6], erosion[7], shallow groundwater rise[8] and subsidence[9].

Ocean storms amplify coastal hazards due to the compounding effects of storm surge[10], wave setup and run-up[11], rainfall[12], and/or elevated river flows[13]. Climate change is predicted to alter these processes, which increase nonlinearly with SLR and rising ocean temperatures[5,14].

Beaches are often the first line of defence against coastal flooding, providing protection for residents and infrastructure. However, beach loss and related inundation (that is, permanent flooding[15]) may be substantial in the coming decades, as SLR drives shorelines inland, with beaches often narrowing due to reduced coastal sediment

[1]Pacific Coastal and Marine Science Center, U.S. Geological Survey, Santa Cruz, CA, USA. [2]Department of Geosciences, University of Arkansas, Fayetteville, AR, USA. [3]Earth Resources Observation & Science Center, U.S. Geological Survey, Sioux Falls, SD, USA. [4]Deltares, Delft, Netherlands. [5]Engineer Research and Development Center, U.S. Army Corps of Engineers, Vicksburg, MS, USA. [6]Deltares USA, Silver Spring, MD, USA. [7]Department of Geosciences, Virginia Tech, Blacksburg, VA, USA. [8]Water Research Laboratory, School of Environmental and Civil Engineering, UNSW Sydney, Manly Vale, New South Wales, Australia. [9]Western Geographic Science Center, U.S. Geological Survey, Moffett Field, CA, USA. ✉e-mail: pbarnard@usgs.gov

https://doi.org/10.1038/s41558-024-02180-2

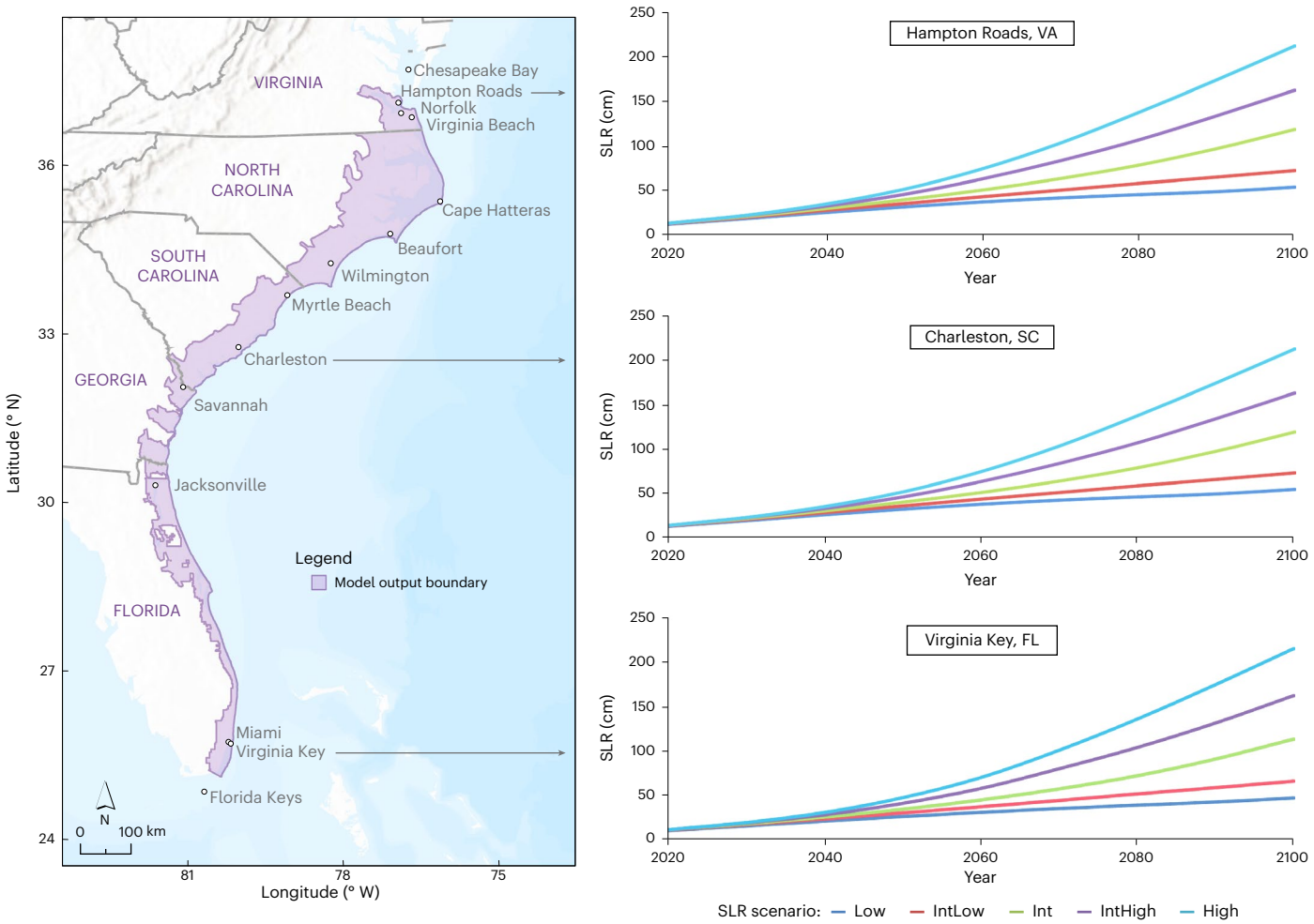

Fig. 1 | Study area. Modelled area and projected SLR[14] along the US Southeast Atlantic coast, which is consistent with the SLR scenarios used in this study. Int, Intermediate. Credit: basemap in **a**, Esri, TomTom, Garmin, FAO, NOAA, USGS, EPA, USGS.

supplies[16] and infrastructure constraining the landward movement of the beach[17,18]. Thus the majority of beaches in urbanized settings may be permanently inundated by 2100, pinned between rising seas and adjacent infrastructure[19,20].

The less visible threat of rising, shallow coastal groundwater as a dynamic coastal hazard has only recently received vigorous attention, but the associated potential exposure and impacts could equal or exceed that of flooding and erosion hazards[8,21,22]. SLR can cause shallow groundwater to rise and emerge at the surface, inundating low-lying coastal regions, which can harm communities in a number of ways, including undermining road and structural foundations, compromising septic systems, mobilizing sequestered or subsurface contaminants, damaging underground utilities, and contaminating soil and groundwater through saltwater intrusion[5,23].

The gradual sinking of land, known as subsidence, poses another potentially severe and complex threat to coastal communities[24,25]. As land subsides, the local relative sea level effectively increases, resulting in a greater inland extent of inundation, as well as episodic storm-driven flooding[26,27]. Anthropogenic activities, such as groundwater extraction, can increase subsidence, adding to the complexity of managing multiple coastal risks[25,28]. Subsidence can directly compromise the structural integrity of affected infrastructure[29], leading to cracked roads, damaged foundations and broken pipelines[30]. The multifaceted nature of subsidence, intertwined with climate change and human activities, makes the gradual sinking of the land a particularly potent hazard in many coastal regions, especially for coastal cities where anthropogenically enhanced subsidence can be acute[31] and contribute to relative SLR and associated hazards[32].

The East Coast of the United States is particularly susceptible to exposure from a suite of coastal hazards driven by both storms and SLR because it is a low-gradient, passive coastal margin comprising numerous low-relief, heavily populated barrier islands that are exposed to large waves and storm surge from tropical and extratropical storms. The East Coast has endured some of the most frequent and costly tropical storm impacts in the United States[33,34], with the section south of Chesapeake Bay and north of the Florida Keys—the focus of this study—recording the most hurricane landfalls. Recent high-impact events include Hurricane Sandy (2012), Hurricane Matthew (2016), Hurricane Florence (2018) and Hurricane Dorian (2019), which together caused over US$125 billion (2023 dollars) in damages[33]. Observational evidence from the past few decades suggests that tropical cyclones in the North Atlantic Ocean have been increasing in frequency and intensity[35,36], and these increases are projected to continue with climate change[37].

In addition to hurricane-related impacts, the US Southeast Atlantic coast also has anomalously high rates of SLR, further increasing hazard exposure. The coastline stretching for 1,000 km north of Cape Hatteras has been a hotspot for decades, with SLR accelerating ~3–4 times faster than the global average from 1970 to 2009[38]. South of Cape Hatteras, observed SLR rates of >10 mm yr^{-1} have been attributed to internal variability over multi-annual/decadal time scales[39]. These observations have been linked to the variability of the North Atlantic Oscillation[40,41] and Florida Current dynamics[42,43], and have been the

cause of a rapid increase in the frequency of nuisance flooding over the past few decades[14].

Here, we quantify socioeconomic exposure of communities across the US Southeast Atlantic coast (Norfolk, Virginia, to Miami, Florida; Fig. 1), home to 14 million residents, to four coastal hazards: flooding, shallow and emerging groundwater, beach erosion, and subsidence, across a range of plausible twenty-first-century SLR[14,44] and storm scenarios. Results demonstrate that population and property exposure to shallow groundwater hazards is comparable in magnitude to flood hazards and that erosion and subsidence may also substantially affect coastal communities, indicating that climate adaptation planning may require a more holistic approach that includes this broader range of coupled, coastal hazards.

Results

The coastal hazard zones used to project coastal community exposure to SLR and storms[45] across the US Southeast Atlantic coast are based on the Coastal Storm Modeling System (CoSMoS[6]). CoSMoS is a modelling framework (Supplementary Fig. 1 and Supplementary Table 1) that integrates observations, global climate models[46] and a series of state-of-the-art oceanographic models for tides, waves and storm surge to assess compound flooding[6], erosion[18] and shallow groundwater hazards[22] for the twenty-first century in the coastal zone. For more information on the approach, including model validation and uncertainty (for example, 95% confidence interval) for the flooding, erosion and groundwater models, see Methods.

Variations in the type and extent of coastal hazards addressed here are visualized at both a regional scale and for one coastal section in the city of Miami Beach, Florida (Fig. 2). Hazard zones for the 1.00 m SLR scenario are utilized for both sets of maps (except vertical land motion (VLM)), which are consistent with the Intermediate SLR projection by 2100 for the region[14]. The regional map (Fig. 2a) demonstrates that coastal hazard zones are estimated to extend far inland. The localized maps of Miami Beach (Fig. 2b–e) display more detail on the extent of these hazard zones; for example, 1.00 m of SLR is predicted to result in either very shallow groundwater (<1 m from the land surface) or daily flooding (that is, primarily driven by SLR and high tides) for the entire community. Hazard exposure is expected to be further magnified by the projected shoreline retreat (absent additional shoreline stabilization via coastal armouring or increased beach nourishment) and land subsidence, which are of the order of 200 m and 1–2 mm yr^{-1}, respectively. These are not accounted for in the median flood hazard zones, but are incorporated in the flooding uncertainty (Methods). This pattern of coastal hazard exposure is projected to be similar for many of the low-lying population centres in the region during the twenty-first century, including Jacksonville, Savannah, Charleston, Wilmington, Beaufort and Virginia Beach (locations provided in Fig. 1).

Flooding

Within our study area, model results project that the extent of daily flooding will increase substantially as SLR continues to increase. The number of residents exposed daily increases from approximately 180,000, assuming 0.25 m of SLR (predicted by ~2050 under most scenarios[14]), to >0.5 million people, assuming 1.00 m of SLR (predicted by ~2100 under the Intermediate scenario[14]; Fig. 3a). For the same scenarios, the estimated value of property within the flood hazard zones increases from ~US$18 to US$80 billion (Supplementary Fig. 2a).

Storm-driven flooding under present sea level represents a substantial threat to many coastal residents, with ~4 and 6 million people in flood hazard zones assuming 20- and 100-year storms based on global climate models (Methods), respectively (Fig. 3a). The addition of SLR substantially increases the extent of storm-related flood hazard zones, particularly for the annual storm, resulting in population exposure estimates increasing more than three times with 1.00 m of SLR, and nearly ten times for 2.00 m of SLR. By 2100, assuming 1.00 m of SLR, the number of residents in coastal flooding hazard zones is projected to be 1.4, 5.6 and 7.0 million assuming annual, 20-year and 100-year storms, respectively. The same scenarios result in US$212 billion, US$626 billion and US$768 billion in property exposure, respectively (Supplementary Fig. 2a). More than 9 million residents (64% of the coastal population in the study area) and US$1 trillion in property are in areas that could experience flooding with 3.00 m of SLR and a 100-year storm.

Shallow groundwater

Areas with shallow and emerging groundwater (that is, water table <2 m from land surface) are estimated to contain ~10 million residents (Fig. 3b) and US$1 trillion in property (Supplementary Fig. 2b), assuming 1.00 m of SLR. Exposure to such groundwater hazards declines under the higher SLR scenarios (that is, 1.50, 2.00 and 3.00 m) because daily flooding becomes increasingly more pervasive in low-lying coastal areas. The areal extent of the coastal groundwater hazard does not increase with rising sea levels, instead dropping ~10% from present-day conditions (23,548 km^2) to 1.00 m of SLR (21,167 km^2; Supplementary Table 2). The groundwater hazard zone does migrate slowly to higher elevations but loses area along the seaward edge because the extent of daily flooding increases by three times during that same interval, leading to the expanded inundation of low-lying areas.

Erosion

The median shoreline recession by 2100 along the US Southeast Atlantic coast due to 1.00 m of SLR (Fig. 4a) under the unimpeded model case (that is, where the shoreline is assumed to be undefended, and allowed to migrate without constraint into backbeach vegetation, infrastructure and developed areas) is approximately 107 m (relative to the initial shoreline state ca. 1990), with a large degree (±157 m, where ± represents standard deviation) of alongshore variability. Future erosion is projected to be the most severe on the small barrier islands of Georgia, South Carolina and Virginia, as much as twice the median projected erosion of the entire study area (Fig. 4a). When shoreline migration is impeded or constrained by the landward end of the modern-day beach (that is, a case that assumes that urban infrastructure, coastal defence structures and/or vegetation fixes the currently existing location of the backbeach), the median shoreline recession is approximately 50 m (±98 m); however, sections of sandy beach can become lost or permanently inundated (Fig. 4b). The loss of the sandy beach due to shoreline recession adjacent to a constrained urban hardscape or backbeach vegetation (that is, the migration-impeded model case) under 1.00 m of SLR is projected for 65–88% of the study area, including 94% of the beaches along the Outer Banks of North Carolina. The model includes the shoreline stabilizing effects of local beach nourishments via a data-assimilated residual shoreline trend (Methods), and the results presented here suggest that current rates of nourishment are insufficient to keep pace with accelerated SLR-driven recession.

The likelihood of projected beach loss/drowning for the migration-impeded model case and the 1.00 m SLR scenario (as a function of time) and as a function of different SLR scenarios, for example, 0.25, 0.50 and 0.75 m (which are assumed to occur prior to 2100), and 1.00, 1.50, 2.00, 2.50 and 3.00 m at 2100, are presented in Fig. 5. Under 1.00, 2.00 and 3.00 m of SLR by 2100 and including consideration of uncertainty, 65, 95 and 99% of beaches, respectively, are likely to erode past the landward end of the existing sandy beach.

The number of residents in areas predicted to erode under the migration-impeded model case (for example, ~11,000 residents for the 1.00 m SLR scenario) is about 1–3 orders of magnitude less than in areas affected by shallow groundwater and flooding hazards (Fig. 3c). However, the unimpeded model case indicates an increase in the population exposed to erosion, and resulting inundation, for all future SLR scenarios (for example, ~36,000 residents for the 1.00 m scenario), including about an order of magnitude increase in exposure for the higher SLR scenarios (that is, 1.50, 2.00 and 3.00 m).

https://doi.org/10.1038/s41558-024-02180-2

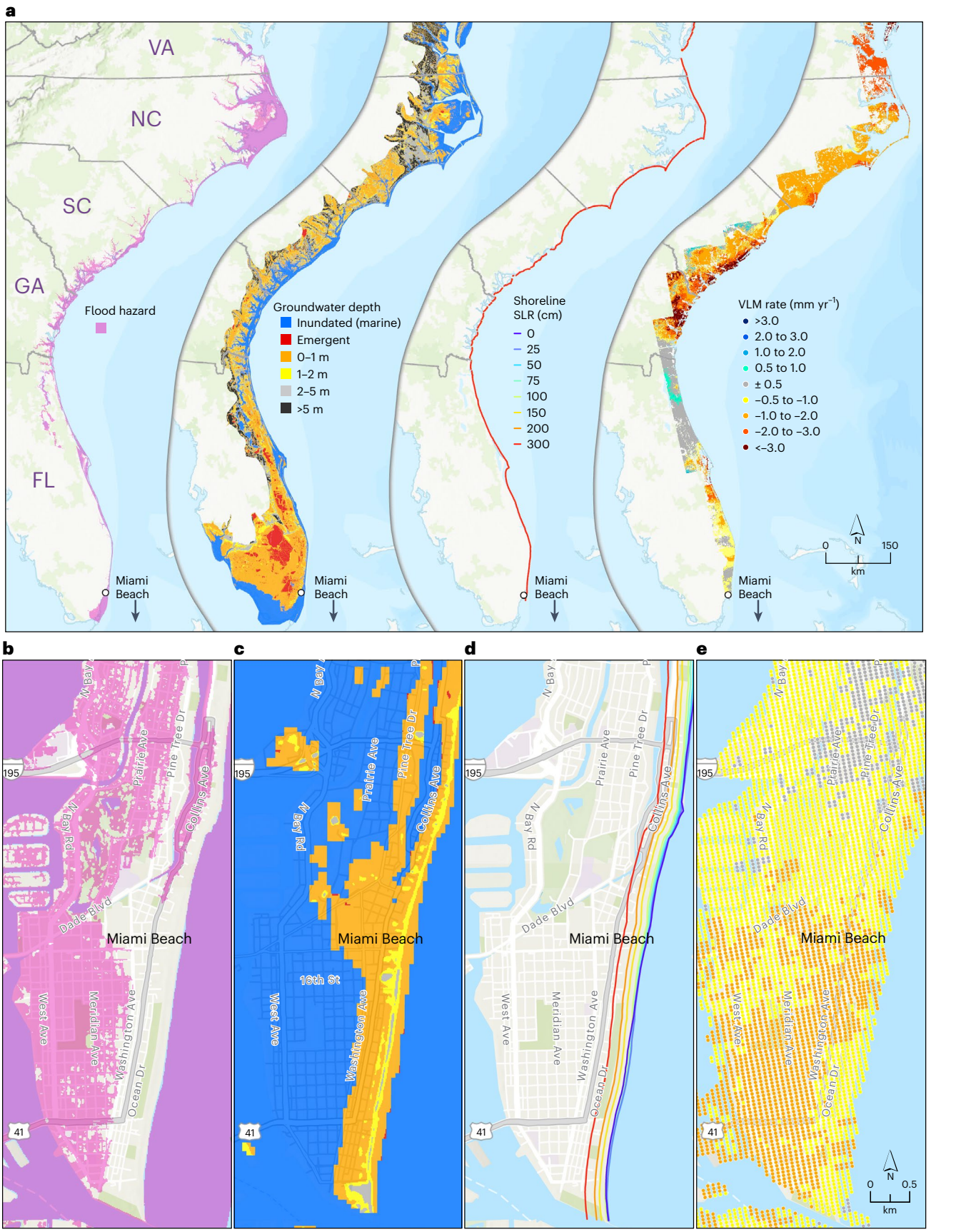

Fig. 2 | Coastal hazard exposure across the study area. a, Coastal flooding (no storm), shallow groundwater exposure and erosion (unimpeded model case) for 1.00 m of SLR (that is, the Intermediate scenario projected for 2100[14]), and observed VLM across the Southeast Atlantic coast. **b**–**e**, A section of the city of Miami Beach showing coastal flooding (no storm; **b**), shallow groundwater exposure (**c**) and erosion (unimpeded model case) for 1.00 m of SLR (**d**) and observed VLM (**e**). Credit: basemaps, Esri, TomTom, Garmin, FAO, NOAA, USGS, EPA, USGS.

https://doi.org/10.1038/s41558-024-02180-2

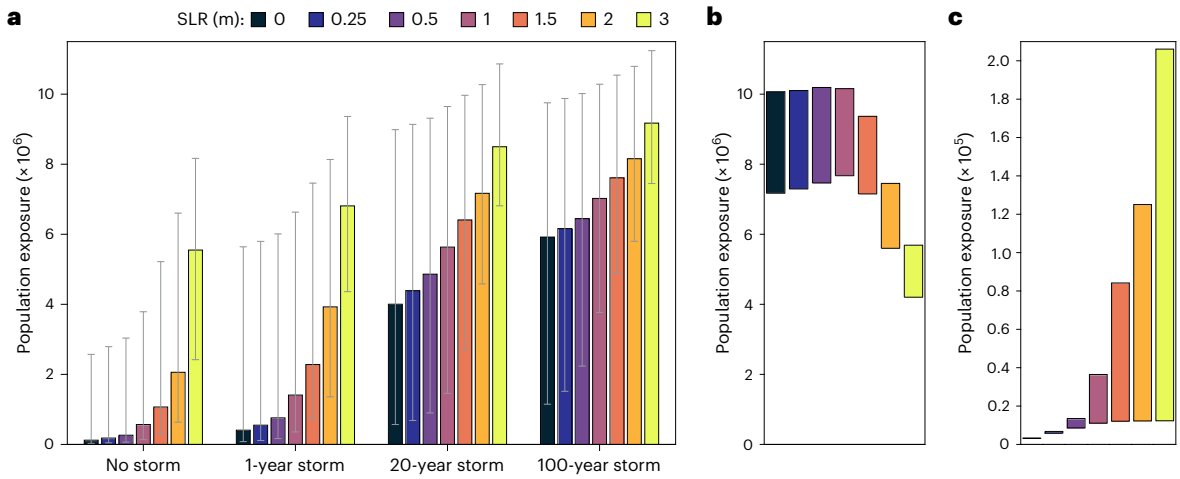

Fig. 3 | Population exposure (based on 2020 US Census) across the Southeast Atlantic coast study area. a, Median flooding exposure for each of the 28 SLR and storm scenarios, with minimum and maximum error bounds (grey bars) based on a 95% confidence interval. **b**, Shallow groundwater hazard exposure for each SLR scenario, with the bars showing the number of residents living in areas where the water table is <1 m (bottom of bar) and <2 m (top of bar) from the ground surface. **c**, Erosion hazard exposure, with each bar showing the range of retreat from assuming shoreline migration is limited to the landward edge of the present-day beach (impeded model case, bottom of bar, lower population exposure) to assuming the shoreline is allowed to migrate landward beyond the landward edge of the present-day beach (unimpeded model case, top of bar, higher population exposure).

Subsidence

The spatial pattern of vertical land motion (VLM) within the study area indicates extensive and variable subsidence, exceeding 4 mm yr^{-1} in some coastal regions of Virginia, North and South Carolina, and Georgia (Fig. 2). Conversely, the northeast section of Florida displays a relatively stable pattern of ground motion. Cities exposed to notable subsidence in the region include Miami, Savannah, Charleston, Myrtle Beach, Virginia Beach, Hampton Roads and Norfolk. Across the region, 1.3 million residents currently live in areas where subsidence exceeds 2 mm yr^{-1} (ref. 27).

Discussion

The number of residents and total parcel value of property in areas predicted to be exposed to coastal hazards in the study area under future climate change scenarios[14,44] is substantial, based on our data-assimilation techniques and modelling approaches. Shallow, emerging coastal groundwater is a hazard that is at least broadly comparable in terms of socioeconomic exposure to flooding. For example, with 1.00 m of SLR (expected by 2100 under the Intermediate SLR scenario[14]), ~70% of existing coastal residents and US$1 trillion in property could be exposed to shallow (that is, water table <2 m from land surface) and emerging groundwater, more than an order of magnitude greater exposure than to daily flooding. Storms dramatically increase flooding exposure. Including the 100-year storm increases population exposure to flooding for the 0.25 m SLR case (expected ~2050) more than 30 times over no-storm (daily tidal) conditions, and more than 10 times for the 1.00 m SLR case. In addition, with 1.00 m of SLR, shorelines are projected to migrate approximately 50 m inland if landward beach migration is restricted by fixing the present-day backbeach location (that is, impeded model case) with coastal defence structures, leading to the potential loss of ~80% of modern beaches within the study area. Pervasive subsidence is also observed and expected to continue across broad regions of the study region, which would further exacerbate flooding and shallow groundwater hazards.

Exposure to daily flooding is projected to double in the study area for every 50 cm of SLR within the 0–2.00 m range of SLR scenarios. More than 5.5 million coastal residents could be exposed to daily flooding with 3.00 m of SLR, which could occur as early as 2120 under the High SLR scenario[14]. This increase in population exposure is approximately 30 times higher than estimates for the more near-term 0.25 m SLR scenario, which is projected to occur between 2030 and 2050 across the Southeast Atlantic coast[14]. Population exposure to coastal hazards also could be higher by extrapolating historical rates of population growth, which has been estimated to be a 3–4 times increase by 2100 for the coastal counties in our study area[47]. Assuming historical rates of population growth, the estimates of 10 million residents exposed to groundwater hazards with 1.00 m of SLR at 2100 therefore could rise to 40 million residents. Hazard exposure estimates that include population projections assuming historical growth rates, however, may not be realistic as they do not consider the land capacity of already highly developed coastal zones, and additional factors could result in a wide range of potential population trajectories (Methods)[48].

This study assessed the influence of end-member shoreline management options, that of restricting the landward migration of the shoreline (or not), and the influence of historical rates of beach nourishment on future shoreline behaviour, but assumes no changes in past anthropogenic activities. The results demonstrate that the historical rate of beach nourishment will have minimal influence on regional shoreline projections. Restricting landward shoreline migration through backbeach hardening (for example, seawalls, revetments) will probably result in the loss of 80% of beaches with 1.00 m of SLR, although allowing the shoreline to migrate landward would expose more than three times the population to land loss and inundation. This presents a challenge to coastal managers, who have to weigh the benefits of defending the shoreline to protect residents and infrastructure at the expense of widespread beach loss, or allow the shoreline to naturally migrate landward with SLR to preserve beaches and associated ecosystems, but with socioeconomic consequences.

Quantifying the influence of future human interventions on coastal hazard exposure is challenging at the regional scale, as management response to future risk is decided locally, and is shaped by unique social values and systems, such as local demographics, economics, governance structures, policies and historical discriminatory practices (for example, redlining). Capturing the complexities of possible local management actions in a computationally expensive modelling approach at the regional scale of this study was outside the scope. The interactions of social and hydrological systems present a promising field of research[49–51], but are not thoroughly addressed here.

Groundwater hazards continue to be challenging to translate into tangible coastal risk and associated socioeconomic impacts as exposure

https://doi.org/10.1038/s41558-024-02180-2

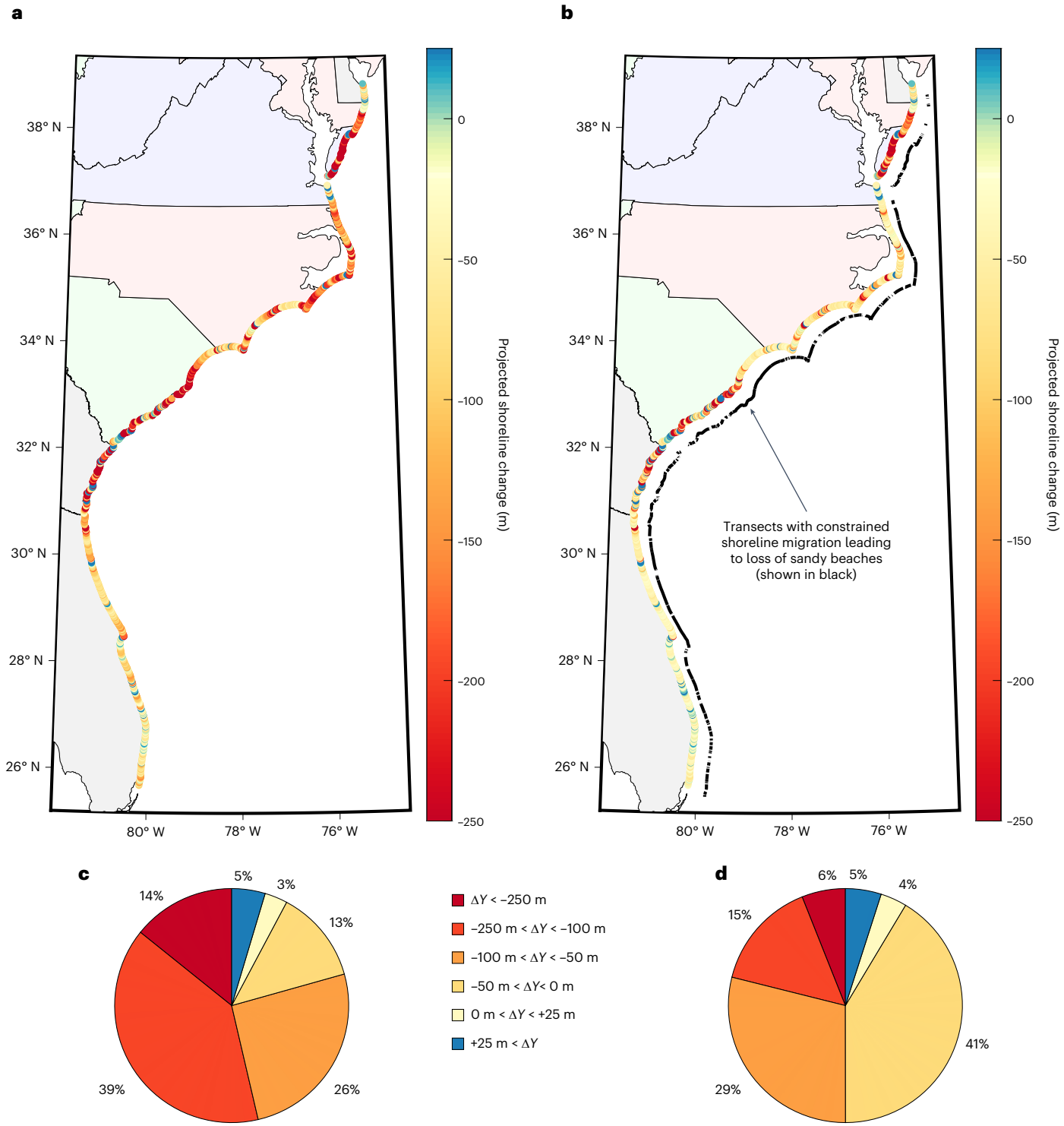

Fig. 4 | Projected shoreline change. Model-projected shoreline change (ΔY) by 2100 relative to the initial shoreline state (ca. 1990) due to 1.00 m of SLR along the US Southeast Atlantic coast (negative values indicate erosion and positive values indicate accretion). **a**, Projected shoreline for the unimpeded model case where the shoreline is allowed to migrate beyond the landward edge of the present-day beach. **b**, Impeded model case where shoreline migration is limited/constrained to the landward edge of the present-day beach. **c**,**d**, Pie charts under the unimpeded (**c**) and migration-impeded (**d**) model cases, which show categorical descriptions of shoreline change magnitudes (for example, >25 m of accretion, 0–50 m of erosion and so on), and the associated percentages across the entire Southeast Atlantic model domain. Basemaps in **a** and **b** created with MATLAB.

to shallow and emerging groundwater is variable, and data are limited[52]. For example, impacts of shallow groundwater depend on the types of buried infrastructure or contaminated soils, and the groundwater hazard is most consequential in areas where buried infrastructure was originally designed for unsaturated conditions, such as buildings, roadbeds[53] and septic leach fields[54], or where larger drain pumps would be required to remove excess water (for example, subways, airports, filled wetlands). One of the challenges for comparing groundwater to flooding hazards is that a thorough accounting of underground infrastructure is much more difficult to acquire than above-ground infrastructure, and there

https://doi.org/10.1038/s41558-024-02180-2

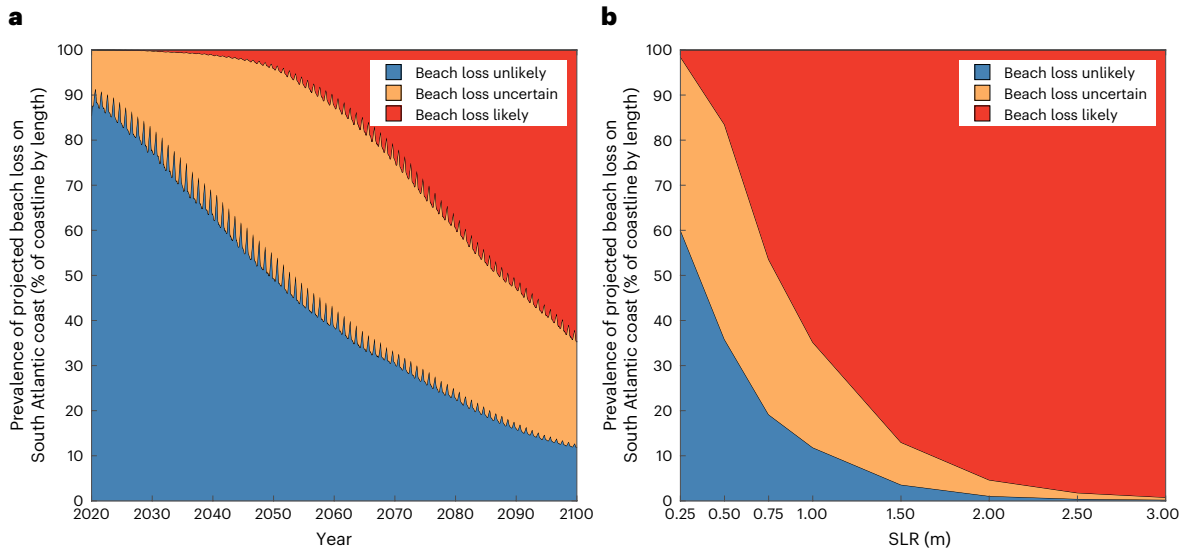

Fig. 5 | Projected beach loss. a,**b**, Projected beach loss (%) when shoreline migration is impeded/constrained to not erode past the present-day dividing line between sandy beach and urban infrastructure or vegetation for the Southeast Atlantic coast as a function of time for the 1.00 m SLR scenario (**a**) and as a function of different SLR scenarios, for example, 0.25, 0.50 and 0.75 m, which are assumed to occur prior to 2100, and 1.00, 1.50, 2.00, 2.50 and 3.00 m assumed to occur at 2100 (**b**). The blue, orange and red portions of the figure correspond to low, medium and high likelihood of beach loss, respectively, where low likelihood of beach loss indicates where the upper bound of erosion potential (that is, the maximum landward limit of the model projections plus uncertainty)[18] is seaward of the present-day infrastructure/vegetation boundary; medium likelihood of beach loss shows where infrastructure/vegetation boundary falls between the upper and lower uncertainty bound of erosion potential; and high likelihood of beach loss is where the infrastructure/vegetation boundary is seaward of the lower uncertainty bound of potential erosion.

are no standard depth–damage functions like those that have existed for decades based on extensive building inventories[55]. This study clearly demonstrates that shallow and emerging coastal groundwater is a hazard that is at least broadly comparable in exposure risk and potential socioeconomic impacts to flooding. For the lower SLR scenarios (that is, through 1.00 m of SLR), the population exposure to shallow groundwater is many times higher than for daily flooding and is projected to affect ~70% of the coastal population in the study area; not until 3.00 m of SLR is population exposure projected to be comparable for groundwater and daily flooding (~5.5 million residents each), and at that time hundreds of thousands of people will transition from being exposed to shallow groundwater hazards to potentially more undesirable flooding hazards.

Subsidence in recent decades has already increased flood frequency across the region[14], particularly in urban centres where extensive development within reclaimed estuaries and/or groundwater pumping locally accentuates the regional downward signal[27]. In addition to increasing SLR-driven flood risk, subsidence is negatively impacting coastal ecosystems by increasing the rate of drowning of tidal wetlands and the development of ghost forests[56]. As global SLR accelerates, impacts can be mitigated if the causes of subsidence are recognized and addressed in climate adaptation planning.

All the above hazards not only impact human populations and associated infrastructure, but also can stress coastal ecosystems. Tidal wetlands and sandy beaches are already particularly vulnerable[57] due to a range of anthropogenic stressors, including land conversion[58,59] and shoreline armouring[60], and projected SLR will further challenge ecosystem sustainability[61–63]. Tidal wetlands often attenuate storm-driven flooding by absorbing flood waters[64–66], and therefore continued wetland deterioration would increase coastal flood risk. The potential loss of up to 80% of modern-day Southeast Atlantic coast beaches, due to rising seas and hardened infrastructure limiting the landward extent of beach migration along urbanized coasts (that is, coastal squeeze[20]), will also stress more landward coastal ecosystems, as the storm protection that beaches provide will be reduced for adjacent dunes, forests and tidal wetlands.

Despite uncertainties in the rate of future population growth, management actions, model accuracy or the ultimate trajectory of SLR (Methods), the percentage of the current population estimated to be affected by coastal hazards along this low-lying, passive margin coast is substantial. Hazard events of this scale (for example, riverine flooding, wildfires, coastal flooding, earthquakes) also have cascading impacts across regions, including indirect economic losses due to interruptions and/or complete failures in transportation infrastructure, communication networks and employment, as well as effects on property values, tax revenues and hazard insurance rates[67]. In addition, public utility disruptions, such as electricity, gas and water supplies, can have short- and long-term consequences on public health[68]. For the Southeast Atlantic coast, where up to 50% of the current population will be at risk of coastal flooding during storms over the next century, and 70% to shallow groundwater hazards, both of which will be further amplified by beach erosion and subsidence, the direct and cascading impacts of SLR- and storm-driven hazards could be severe. Effective climate adaptation planning would consider this confluence of hazards together as communities invest in resilience strategies to protect life and property along this vulnerable stretch of the US coast, which is representative of low-lying coastal communities across the world.

Online content

Any methods, additional references, Nature Portfolio reporting summaries, source data, extended data, supplementary information, acknowledgements, peer review information; details of author contributions and competing interests; and statements of data and code availability are available at https://doi.org/10.1038/s41558-024-02180-2.

References

1. Neumann, B., Vafeidis, A. T., Zimmermann, J. & Nicholls, R. J. Future coastal population growth and exposure to sea-level rise and coastal flooding—a global assessment. *PLoS ONE* **10**, e0118571 (2015).
2. Kulp, S. A. & Strauss, B. H. New elevation data triple estimates of global vulnerability to sea-level rise and coastal flooding. *Nat. Commun.* **10**, 4844 (2019).

3. Hauer, M. E. et al. Sea-level rise and human migration. *Nat. Rev. Earth Environ.* **1**, 28–39 (2020).
4. Taherkhani, M. et al. Sea-level rise exponentially increases coastal flood frequency. *Sci. Rep.* **10**, 6466 (2020).
5. May, C. L. et al. in *Fifth National Climate Assessment* (eds Crimmins, A. R. et al.) Ch. 9 (US Global Change Research Program, 2023).
6. Barnard, P. L. et al. Dynamic flood modeling essential to assess the coastal impacts of climate change. *Sci. Rep.* **9**, 4309 (2019).
7. Hinkel, J. et al. A global analysis of erosion of sandy beaches and sea-level rise: an application of DIVA. *Glob. Planet. Change* **111**, 150–158 (2013).
8. Rotzoll, K. & Fletcher, C. H. Assessment of groundwater inundation as a consequence of sea-level rise. *Nat. Clim. Change* **3**, 477–481 (2013).
9. Allison, M. et al. Global risks and research priorities for coastal subsidence. *Eos* **97**, 22–27 (2016).
10. Tebaldi, C., Strauss, B. H. & Zervas, C. E. Modelling sea level rise impacts on storm surges along US coasts. *Environ. Res. Lett.* **7**, 014032 (2012).
11. Stockdon, H. F. et al. Operational forecasts of wave-driven water levels and coastal hazards for US Gulf and Atlantic coasts. *Commun. Earth Environ.* **4**, 169 (2023).
12. Rahimi, R., Tavakol-Davani, H., Graves, C., Gomez, A. & Valipour, M. F. Compound inundation impacts of coastal climate change: sea-level rise, groundwater rise and coastal precipitation. *Water* **12**, 2776 (2020).
13. Moftakhari, H. R., Salvadori, G., AghaKouchak, A., Sanders, B. F. & Matthew, R. A. Compounding effects of sea level rise and fluvial flooding. *Proc. Natl Acad. Sci. USA* **114**, 9785–9790 (2017).
14. Sweet, W. V. et al. *Global and Regional Sea Level Rise Scenarios for the United States: Updated Mean Projections and Extreme Water Level Probabilities Along U.S. Coastlines* NOAA Technical Report NOS 01 (NOAA, National Ocean Service, 2022).
15. Flick, R. E., Chadwick, D. B., Briscoe, J. & Harper, K. C. 'Flooding' versus 'inundation'. *Eos* **93**, 365–366 (2012).
16. Slagel, M. J. & Griggs, G. B. Cumulative losses of sand to the California coast by dam impoundment. *J. Coast. Res.* **24**, 571–584 (2008).
17. Lentz, E. E. et al. Evaluation of dynamic coastal response to sea-level rise modifies inundation likelihood. *Nat. Clim. Change* **6**, 696–700 (2016).
18. Vitousek, S., Vos, K., Splinter, K. D., Erikson, L. & Barnard, P. L. A model integrating satellite-derived shoreline observations for predicting fine-scale shoreline response to waves and sea-level rise across large coastal regions. *J. Geophys. Res. Earth Surf.* **128**, e2022JF006936 (2023).
19. Vousdoukas, M. I. et al. Sandy coastlines under threat of erosion. *Nat. Clim. Change* **10**, 260–263 (2020).
20. Pontee, N. Defining coastal squeeze: a discussion. *Ocean Coast. Manag.* **84**, 204–207 (2013).
21. Sukop, M. C., Rogers, M., Guannel, G., Infanti, J. M. & Hagemann, K. High temporal resolution modeling of the impact of rain, tides and sea level rise on water table flooding in the Arch Creek basin, Miami-Dade County Florida USA. *Sci. Total Environ.* **616–617**, 1668–1688 (2018).
22. Befus, K. M., Barnard, P. L., Hoover, D. J., Finzi Hart, J. A. & Voss, C. I. Increasing threat of coastal groundwater hazards from sea-level rise in California. *Nat. Clim. Change* **10**, 946–952 (2020).
23. Hill, K., Hirschfeld, D., Lindquist, C., Cook, F. & Warner, S. Rising coastal groundwater as a result of sea-level rise will influence contaminated coastal sites and underground infrastructure. *Earth's Future* **11**, e2023EF003825 (2023).
24. Cao, A. et al. Future of Asian deltaic megacities under sea level rise and land subsidence: current adaptation pathways for Tokyo, Jakarta, Manila and Ho Chi Minh City. *Curr. Opin. Environ. Sustain.* **50**, 87–97 (2021).
25. Shirzaei, M. et al. Measuring, modelling and projecting coastal land subsidence. *Nat. Rev. Earth Environ.* **2**, 40–58 (2021).
26. Brown, S. & Nicholls, R. J. Subsidence and human influences in mega deltas: the case of the Ganges–Brahmaputra–Meghna. *Sci. Total Environ.* **527–528**, 362–374 (2015).
27. Ohenhen, L. O., Shirzaei, M. & Barnard, P. L. Slowly but surely: exposure of communities and infrastructure to subsidence on the US East Coast. *Proc. Natl Acad. Sci. Nexus* **3**, pgad426 (2024).
28. Candela, T. & Koster, K. The many faces of anthropogenic subsidence. *Science* **376**, 1381–1382 (2022).
29. Parsons, T., Wu, P.-C., Wei, M. & D'Hondt, S. The weight of New York City: possible contributions to subsidence from anthropogenic sources. *Earth's Future* **11**, e2022EF003465 (2023).
30. Ohenhen, L. O. & Shirzaei, M. Land subsidence hazard and building collapse risk in the coastal city of Lagos, West Africa. *Earth's Future* **10**, e2022EF003219 (2022).
31. Wu, P.-C., Wei, M. & D'Hondt, S. Subsidence in coastal cities throughout the world observed by InSAR. *Geophys. Res. Lett.* **49**, e2022GL098477 (2022).
32. Ohenhen, L. O., Shirzaei, M., Ojha, C., Sherpa, S. F. & Nicholls, R. J. Disappearing cities on US coasts. *Nature* **627**, 108–115 (2024).
33. *U.S. Billion-Dollar Weather and Climate Disasters* (NOAA National Centers for Environmental Information, 2023); https://www.ncei.noaa.gov/access/billions/
34. *Continental United States Hurricane Impacts/Landfalls 1851–2022* (NOAA Hurricane Research Division, 2023); https://www.aoml.noaa.gov/hrd/hurdat/All_U.S._Hurricanes.html
35. Klotzbach, P. J. et al. Trends in global tropical cyclone activity: 1990–2021. *Geophys. Res. Lett.* **49**, e2021GL095774 (2022).
36. Garner, A. J. Observed increases in North Atlantic tropical cyclone peak intensification rates. *Sci. Rep.* **13**, 16299 (2023).
37. Balaguru, K. et al. Increased U.S. coastal hurricane risk under climate change. *Sci. Adv.* **9**, eadf0259 (2023).
38. Sallenger, A. H., Doran, K. S. & Howd, P. A. Hotspot of accelerated sea-level rise on the Atlantic coast of North America. *Nat. Clim. Change* **2**, 884–888 (2012).
39. Dangendorf, S. et al. Acceleration of U.S. Southeast and Gulf coast sea-level rise amplified by internal climate variability. *Nat. Commun.* **14**, 1935 (2023).
40. Ezer, T., Atkinson, L. P., Corlett, W. B. & Blanco, J. L. Gulf Stream's induced sea level rise and variability along the U.S. mid-Atlantic coast. *J. Geophys. Res. Ocean* **118**, 685–697 (2013).
41. Valle-Levinson, A., Dutton, A. & Martin, B. Spatial and temporal variability of sea level rise hot spots over the eastern United States. *Geophys. Res. Lett.* **44**, 7876–7882 (2017).
42. Yin, J. & Goddard, P. B. Oceanic control of sea level rise patterns along the East Coast of the United States. *Geophys. Res. Lett.* **40**, 5514–5520 (2013).
43. Domingues, R., Goni, G., Baringer, M. & Volkov, D. What caused the accelerated sea level changes along the U.S. East Coast during 2010–2015?. *Geophys. Res. Lett.* **45**, 13,367–13,376 (2018).
44. IPCC *Climate Change 2021: The Physical Science Basis* (eds Masson-Delmotte, V. et al.) (Cambridge Univ. Press, 2021).
45. Wood, N., Jones, J., Henry, K., Ng, P. & Hou, C. Y. *Hazard Exposure Reporting and Analytics* (USGS, accessed 25 April 2024); https://www.usgs.gov/apps/hera
46. Erikson, L. H. et al. *Ocean Wave Time-Series Data Simulated with a Global-Scale Numerical Wave Model Under the Influence of Projected CMIP6 Wind and Sea Ice Fields* (USGS, 2022); https://doi.org/10.5066/P9KR0RFM

47. Hauer, M. E., Evans, J. M. & Mishra, D. R. Millions projected to be at risk from sea-level rise in the continental United States. *Nat. Clim. Change* **6**, 691–695 (2016).
48. Hauer, M. E. Population projections for U.S. counties by age, sex and race controlled to shared socioeconomic pathway. *Sci. Data* **6**, 190005 (2019).
49. Murray, A. B., Gopalakrishnan, S., McNamara, D. E. & Smith, M. D. Progress in coupling models of human and coastal landscape change. *Comput. Geosci.* **53**, 30–38 (2013).
50. McNamara, D. E., Lazarus, E. D. & Goldstein, E. B. Human–coastal coupled systems: ten questions. *Camb. Prisms Coast. Futures* **1**, e20 (2023).
51. Anarde, K. A., Moore, L. J., Murray, A. B. & Reeves, I. R. B. The future of developed barrier systems—part I: pathways toward uninhabitability, drowning and rebound. *Earth's Future* **12**, e2023EF003672 (2024).
52. Habel, S., Fletcher, C. H., Barbee, M. M. & Fornace, K. L. Hidden threat: the influence of sea-level rise on coastal groundwater and the convergence of impacts on municipal infrastructure. *Annu. Rev. Mar. Sci.* **16**, 81–103 (2024).
53. Knott, J. F., Elshaer, M., Daniel, J. S., Jacobs, J. M. & Kirshen, P. Assessing the effects of rising groundwater from sea level rise on the service life of pavements in coastal road infrastructure. *Transp. Res. Rec.* **2639**, 1–10 (2017).
54. Humphrey, C. P., Iverson, G. & O'Driscoll, M. Nitrogen treatment efficiency of a large onsite wastewater system in relation to water table dynamics. *CLEAN - Soil, Air, Water* **45**, 1700551 (2017).
55. Appelbaum, S. J. Determination of urban flood damage. *J. Water Resour. Plan. Manag.* **111**, 269–283 (1985).
56. Kirwan, M. L. & Gedan, K. B. Sea-level driven land conversion and the formation of ghost forests. *Nat. Clim. Change* **9**, 450–457 (2019).
57. Ganju, N. K. et al. Spatially integrative metrics reveal hidden vulnerability of microtidal salt marshes. *Nat. Commun.* **8**, 14156 (2017).
58. Huang, Y. et al. Marshland conversion to cropland in northeast China from 1950 to 2000 reduced the greenhouse effect. *Glob. Change Biol.* **16**, 680–695 (2010).
59. Pendleton, L. et al. Estimating global 'blue carbon' emissions from conversion and degradation of vegetated coastal ecosystems. *PLoS ONE* **7**, e43542 (2012).
60. Dugan, J. E., Hubbard, D. M., Rodil, I. F., Revell, D. L. & Schroeter, S. Ecological effects of coastal armoring on sandy beaches. *Mar. Ecol.* **29**, 160–170 (2008).
61. Kirwan, M. & Megonigal, J. Tidal wetland stability in the face of human impacts and sea-level rise. *Nature* **504**, 53–60 (2013).
62. Thorne, K. et al. U.S. Pacific coastal wetland resilience and vulnerability to sea-level rise. *Sci. Adv.* **4**, eaao3270 (2018).
63. Barnard, P. L. et al. Multiple climate change-driven tipping points for coastal systems. *Sci. Rep.* **11**, 15560 (2021).
64. Narayan, S. et al. The value of coastal wetlands for flood damage reduction in the northeastern USA. *Sci. Rep.* **7**, 9463 (2017).
65. van Coppenolle, R. & Temmerman, S. A global exploration of tidal wetland creation for nature-based flood risk mitigation in coastal cities. *Estuar. Coast. Shelf Sci.* **226**, 106262 (2019).
66. Fairchild, T. P. et al. Coastal wetlands mitigate storm flooding and associated costs in estuaries. *Environ. Res. Lett.* **16**, 074034 (2021).
67. Hsiang, S. et al. in *Fifth National Climate Assessment* (eds Crimmins, A. R. et al.) Ch. 19 (US Global Change Research Program, 2023).
68. Patterson, D. L., Wright, H. & Harris, P. N. A. Health risks of flood disasters. *Clin. Infect. Dis.* **67**, 1450–1454 (2018).

Methods

Overview

Hazard zones are determined for seven SLR (0, 0.25, 0.50, 1.00, 1.50, 2.00 and 3.00 m; baseline year 2000) and four storm (daily conditions, annual, 20-year and 100-year) scenarios, for a total of 28 scenarios. Compound flooding is modelled using predictions of precipitation, streamflow and oceanic forcing for the given storm conditions (see below). The 0.25, 0.50, 1.00, 1.50, 2.00 and 3.00 m SLR scenarios correspond to the 2100 scenarios from the US Sea Level Rise and Coastal Flood Hazard Scenarios and Tools Interagency Task Force[14], which are derived from the IPCC Sixth Assessment Report[44]. Community and state hazard exposure are then estimated by geospatial overlay with socioeconomic data and provided to the public through the US Geological Survey (USGS) Hazard Exposure Reporting and Analytics web mapping application[45] (www.usgs.gov/apps/hera). Here, we focus primarily on two community exposure metrics: median population exposure, which is based on total residents from the 2020 US Census block-level data, and property values in 2020 US dollars, based on parcel boundaries and total assessed values from the US Department of Homeland Security. Additional metrics for socioeconomic exposure, including the uncertainty bounds, are provided in Supplementary Table 2.

Digital elevation model

Integrated high-resolution topobathymetric digital elevation models (TBDEMs) provide the foundational geospatial base for driving physical processes such as waves, overland flow and erosion. USGS Coastal National Elevation Database (CoNED) 1 m TBDEMs were developed for the coastal regions of Virginia, North Carolina, South Carolina[69] and Georgia[70], from the continental shelf to at least the 10 m topographic contour, using best available topography and bathymetry data from the USGS 3D Elevation Program, the National Oceanographic and Atmospheric Administration (NOAA) and the US Army Corps of Engineers, along with contributions from many external stakeholders[71–73]. For the Carolinas, a thorough evaluation of the accuracy of the TBDEM was evaluated via comparison of grid values with 1,531 co-located NOAA National Geodetic Survey Global Positioning System on Benchmarks control points and 9,120 USGS field survey control points distributed throughout the study area, reporting a root mean square error over the land and nearshore area of 0.35 m (ref. 74). As CoNED TBDEMs were not available for Florida at the time of the study, a combination of the most recent elevation data covering eastern and southern Florida[75–77] were used for model inputs, with a maximum vertical uncertainty (of all datasets) of less than 1 m. CoNED TBDEMs are constructed from multi-source topographic and bathymetric data that are aligned vertically and horizontally to a common reference system[71]. Input data sources are prioritized for integration based on spatial accuracy and temporal frequency, and ranked accordingly. The land/water interface (±10 m) is the most critical area, and green lidar systems, such as the Coastal Zone Mapping and Imaging Lidar, that cross the nearshore interface are valuable for maintaining a seamless transition elevation map from offshore to onshore. Using source spatial metadata and tile index information, input data sources were spatially mosaicked based on priority to create a seamless topobathymetric composite at a 1 m resolution using a linear spatial blending technique (10 pixel overlap) between input source layers. Spatial metadata consists of a group of geospatial polygons that represent the footprint (pixel level detail) of each input data source used in the TBDEM along with the detailed characteristics of each elevation data source. Each regional TBDEM was validated using a rigorous set of ground control points from USGS field surveys and NOAA's National Geodetic Survey.

VLM

VLM rates from 2007 to 2020 were derived with continuous spatial coverage at 50 m resolution for the study area[78]. The VLM rate datasets were produced using multitemporal synthetic aperture radar (SAR) processing of 17 frames from Sentinel-1 and 95 frames from ALOS-1 satellites (ascending orbit geometry), comprising more than 3,000 SAR images. The authors applied the wavelet-based InSAR algorithm[79–82]. The analysis included the detection and elimination of pixels with average coherence less than 0.7 (so-called noisy pixels), correcting for the effect of orbital error[83], reducing the effects of topographically correlated atmospheric phase delay, and spatially uncorrelated DEM error[79,80]. Next, a reweighted least-squares estimation was utilized to determine each pixel's velocities in the line of sight (LOS) direction. A stochastic model was utilized to combine the LOS velocities with 162 global navigation satellite systems to generate the three-dimensional (3D) velocities tied to IGS14 global reference frame. As previously reported[27], almost 80% of the InSAR-based VLM measurements have a standard deviation smaller than 1 mm yr^{-1}, and validation against independent global navigation satellite system observations yields a standard deviation of 0.78 mm yr^{-1} for their differences. Further information on the input parameters for the model, interferograms, the creation of (LOS) velocities and 3D velocity generation can be obtained from ref. 78.

Flood hazards

Coastal flood hazard modelling followed the general CoSMoS framework to project coastal flooding during the twenty-first century[6,84–86] using multiple modelling tiers to translate global and climate-scale forcing to local scale hazards (that is, block scale) to support coastal management decision-making. However, to make CoSMoS applicable to the Southeast Atlantic, modifications to the workflow were implemented to resolve and assess the impacts of tropical cyclones in addition to extratropical events[87–89]. Owing to the importance of compound flooding in the region, pluvial, fluvial and oceanic drivers were used to develop spatial estimates of extreme water levels using the open-source overland flood model, Super-Fast INundation of CoastS (SFINCS[87,90]; see Supplementary Table 1 for a list of forcing data and Supplementary Fig. 1 for the model framework). SFINCS models were set up as previously described[89], with five large model domains covering the full study region. The continuity and momentum water flow calculations were performed on a 200 × 200 m resolution grid to save computational expense and using the native 1 × 1 m resolution DEM as subgrid-derived lookup tables[90] to better resolve flow routing and dune or infrastructure overwash during storm conditions. Maximum dune elevations along the coast were derived from CoNED, cross-checked with ref. 91 and explicitly included in the model as an alongshore weir to preserve dunes as a flow-blocking feature. Flood protective infrastructure (for example, flood walls, levees, storm drain systems and so on) below the model resolution were not similarly included, owing to both the scale of the study and a lack of a comprehensive inventory. While infrastructure characterized in the DEM is accounted for in subgrid lookup tables[92], the model may overpredict impacts in areas where infrastructure is not depicted in the DEM or where narrow flood defences are present[93]. However, as model outputs are post-processed to subgrid features, any overpredictions become disconnected from the final flood surface and are recategorized as a separate data layer. The models were run on high-performance supercomputers at Deltares and the USGS[94]. Models were validated at 24 NOAA tide stations across the study area for the time between 1980 and 2018, using observed 6-min water levels at the stations. An additional 68 locations from the XTide database[95] were used for validation of tidal amplitude and phase. Finally, the models were validated for the landfalling event of Hurricane Florence (near Wilmington, North Carolina, in 2018), using 156 pressure gauges and 396 high-water marks from the USGS. Model results show for Hurricane Florence that for high-water marks in the coastal region there is a mean absolute error of 30 cm with a bias underestimation of 19 cm (ref. 89).

For extratropical storms, regional scale oceanographic forcing was provided by the Global Tide and Surge Model[96–98]. As described in

ref. 88, Global Tide and Surge Model water levels were corrected using a series of signal-specific statistical corrections (for example, tides, non-tidal residual), and combined with wave setup values derived using the ref. 99 parameterization. An ensemble of three Coupled Model Intercomparison Project Phase 6 (CMIP6) models from the High-Resolution Model Intercomparison Project[100–104] were used for the extratropical storms. Tropical cyclones were accounted for by leveraging work by the US Army Corps of Engineers Coastal Hazards System (https://chs.erdc.dren.mil), which includes a large catalogue of synthetic events using the joint probability method and simulated using coupled ADCIRC–SWAN[105,106]. Together these two datasets provided oceanographic forcing in the very nearshore (~2 m depth) as water level boundaries to the SFINCS model. Streamflow and precipitation were included as important drivers of compound flooding in the region. Precipitation was derived from CMIP6 output fields for extratropical storms and by using the Interagency Performance Evaluation Task Force parameterization for tropical cyclones[107]. Streamflow was derived using statistical models[89], relating meteorological variables and National Water Model data[108]. A large catalogue of storms (~1,000) was simulated, with the set intending to cover the full range of possible extreme events, including hurricanes, extratropical storms and precipitation/fluvial-dominated events. Output data from these simulations were maximum water levels at 1 m resolution for each event and across the entire study region.

Finally, extreme water levels were then calculated on a grid cell basis by creating combined recurrence intervals using the probability of exceedance (Supplementary Fig. 1). Recurrence interval flood surfaces were then derived at a variety of SLR and recurrence interval scenarios. Uncertainty was calculated as a sum of contributions, including underlying DEM uncertainty, projected VLM based on SLR (spatially variable per SLR scenario), and uncertainty with the model and model processes (spatially variable, derived from water level return-period curves at each grid point, dependent on scenario). This spatially variable total uncertainty was applied to the final water elevation (per grid point) and extrapolated outward to depict the maximum and minimum potential flood area considering total uncertainty. For more details, see refs. 88,89. The hazard zones for each scenario are available through USGS data releases[109,110] and can also be viewed interactively at www.usgs.gov/apps/hera.

Groundwater hazards

Shallow groundwater levels were modelled using steady-state simulations with MODFLOW-NWT[111] with overlapping model domains to produce continuous outputs for the study area[22]. The SLR scenarios modelled were added to the spatially variable mean higher high-water elevation[112], and the groundwater levels in model cells with a surface elevation at or below the elevation of sea level were held constant at sea level. Hydrogeology was implemented as a one-layer representation of an unconfined groundwater system with cell thickness and hydraulic conductivity derived from models calibrated with well observations[113]. The model grid cell horizontal resolution was 50 × 50 m, and a total of 72 model domains were developed, with overlapping cells to increase model efficiency and merged to create continuous groundwater modelling products. Modelled hydraulic heads were validated with 6,392 well observations for wells known to be in the unconfined aquifer or otherwise shallower than 45.7 m to limit the potential for confined conditions[114]. At these wells, the mean absolute error was 0.6 m and the median absolute error was 0.03 m. Water table depths were calculated at 10 m resolution by subtracting the 50 m resolution groundwater levels from a 10 m resolution elevation model, as groundwater levels are expected to be less variable in space than topography[115]. For the hazard analysis, the depth to water table data were categorized into three elevation ranges: emergent groundwater with the water table at or above the land surface; very shallow groundwater with water tables within 1 m of the land surface (that could be effectively at the land surface in soils with high capillarity); and shallow groundwater with water tables 1–2 m below the land surface that could negatively influence soil contaminants, buried infrastructure or septic system performance. Groundwater level changes with SLR occurring deeper than 2 m below the land surface could still create subsurface hazards, but we focus on the depth ranges where the most damaging groundwater hazards are expected, given the density of buried infrastructure at 0–2 m depths.

Erosion

Long-term shoreline change is simulated with CoSMoS-COAST, a data-assimilated model that integrates longshore and cross-shore transport due to waves and SLR[18,116–118]. The model considers scenarios of backbeach stabilization versus no stabilization (that is, impeded/migration-constrained model case versus unimpeded model case), where shoreline retreat is either prohibited or allowed, respectively, to retreat past the current landward end of the sandy beach, identified by urban development (where present) or vegetation/dune lines (in non-urbanized natural settings). Although the model only explicitly evolves the shoreline position (and not necessarily the beach width in the unimpeded model case, it operates under the 'equilibrium beach profile' assumption that the presence (and approximate widths) of sandy beaches may be preserved in the future if migration (which is predominantly landward due to SLR) is not constrained by backbeach hardscapes.

The CoSMoS-COAST model solves the one-dimensional conservation of sediment volume in the alongshore direction. The model synthesizes several popular individual-process models including: (1) a 'one-line' model for longshore transport; (2) an equilibrium cross-shore beach profile evolution model due to SLR; (3) a long-term residual shoreline trend that represents sources and sinks of sediment; (4) a wave-driven cross-shore equilibrium shoreline change model; and (5) a noise term. For details on each model component, see ref. 18. Processes like overwash/barrier island rollover are not explicitly parameterized in the model, but their effects on shoreline transgression are implicitly included via the equilibrium cross-shore SLR-driven shoreline recession term (2)[119–121].

The Southeast Atlantic application, comprising roughly 34,000 transects (spaced every 50 m in the alongshore direction), spans open-coast sandy beaches from Miami, Florida, to Cape Henlopen, Delaware (Fig. 2). The model is forced with daily hindcasted and projected wave conditions obtained from the ERA5 reanalysis[122] and seven future wave scenarios from the CMIP6 collection of general circulation models[46,100], respectively. Projections of future relative SLR at tide gauge sites (including local VLM) come from ref. 14. The model is calibrated via an ensemble Kalman filter using 25 years of satellite-derived shoreline observations (from 1990 to 2015 and spanning the entire model domain) obtained with the CoastSat toolbox[123]. After calibration, the model is validated using 5 years of satellite-derived shorelines observations (from 2015 to 2020). The validation period assesses that the model achieves a median root mean square accuracy of $\sigma_{RMSE} = 12.3$ m across the entire Southeast Atlantic domain. Model uncertainty is assessed in two different ways: (1) by running 200-member model ensembles with varying model parameter estimates obtained via data assimilation[18]; and (2) by calculating the root mean square error (σ) between the model-predicted and satellite-observed shoreline positions at each transect during the 2015–2020 validation period and specifying $\pm 2\sigma$ uncertainty bands surrounding the models' median projections.

In many urban locations in the US Southeast Atlantic, episodic beach nourishments are undertaken to stabilize shorelines and reduce erosion[124]. Beach nourishments are generally apparent within satellite-derived shoreline observations (as spikes/jumps in shoreline position). Thus, when nourishment-influenced shoreline observations are assimilated into the model, they can affect the estimation of the

residual shoreline trend and mask naturally occurring rates of erosion. The model scenarios presented here assume that accretionary trends (due to either natural or nourishment effects) are projected to continue (but not accelerate) into the future. Thus, it appears that historical rates of beach nourishment are insufficient to prevent beach loss due to accelerated SLR in the latter half of the twenty-first century (Fig. 5).

Socioeconomic exposure metrics

Socioeconomic exposure to coastal erosion, flooding and groundwater hazard zones for 28 SLR and storm scenarios discussed in previous sections was estimated by the geospatial overlay of population and community asset data[125]. Exposure is based on the spatial coincidence of a hazard zone and a census block or asset. The sensitivity and adaptive capacity of people or assets in hazard zones are not addressed, nor are indirect impacts that could negatively affect assets outside the hazard zones. For this study we focus primarily on two exposure metrics: total residents and property values (additional metrics and uncertainty bounds in Supplementary Table 2). Residential counts are based on 2020 block-level boundaries and total population counts from the US Census Bureau[126] and do not include potential population changes in the future. If census blocks overlapped hazard polygons, final population values were adjusted proportionately using the spatial ratio of each sliver within or outside a hazard zone. For example, if a census block contains ten people and half of the block is in a hazard zone, then we assume that five residents are in the zone. Note that population projections based simply on historical rates of growth are often unrealistic due to development constraints. Furthermore, those projections are typically estimated at county scales; therefore, the extent to which new development will occur homogenously across a county is not assured. Instead, new development may occur in more inland and undeveloped areas of coastal counties, as opposed to areas currently susceptible to coastal hazards, which already may be built out or may have land-use plans that limit new development. Furthermore, populations in US coastal states may remain flat or even decrease if one uses Shared Socioeconomic Pathway Scenarios 3 and 4 developed for the Sixth Assessment Report of the IPCC[48]. Given the wide range of possible population trajectories in coastal communities over the next century, we estimate population exposure to SLR-related coastal hazards using present-day magnitudes and distributions of coastal populations in our study area.

Property values are based on parcel boundaries and their total assessed values (tax year 2020) from LightBox (https://www.lightboxre.com), which provides access to the Homeland Infrastructure Foundation-Level Data[127]. Exposure estimates are available at the state level for Florida[128], Georgia[129], South Carolina[130], North Carolina[131] and Virginia[132]. Estimates of developed land are based on high-, medium- and low-intensity developed classes in the 2016 National Land Cover Database[133]. All socioeconomic exposure estimates (for example, employees, land-use types, critical facilities) are provided in an interactive web application (www.usgs.gov/apps/hera)[46].

Study limitations

A limitation of this study is the lack of consideration for potential feedback mechanisms between the different components. For example, incorporating morphological changes from shoreline changes into the coastal flood modelling would probably further increase flood exposure[6]. Shallower groundwater would reduce infiltration capacity during precipitation events, thereby increasing the frequency and magnitude of flooding. Subsidence is considered in the flood hazard uncertainty, but direct incorporation of subsidence into flood models would also result in increased flood exposure across much of the study area. While limited coupling of different processes has been successfully accomplished over other large study areas[6,84,134], the computational expense and uncertainty of developing a fully coupled modelling approach that includes feedbacks between all the different processes over such a vast region was untenable. Nevertheless, despite uncertainties, this study provides a more comprehensive and detailed regional assessment of multiple coastal hazards compared with higher-level studies that provide national assessments of various aspects of flood risk, such as SLR and storm surge impacts via bathtub flooding with hydrological connectivity[135], the effects of climate-driven changes in precipitation using hydrological modelling[136], and climate-driven compound flooding including pluvial, fluvial and coastal drivers[137].

Data availability

The following datasets are available at https://doi.org/10.5066/P9W91314 for North and South Carolina, and https://doi.org/10.5066/P9BQQTCI for the remaining study area: projections of coastal flood hazards and flood potential, projections of coastal water depths, projected groundwater head, projected water table depths, projected groundwater emergence and shoaling, nearshore water level, tide and non-tidal residual hindcasts (1979–2016), nearshore water level, tide and non-tidal residual future projections (2016–2050), nearshore parametric wave setup hindcast data (1979–2019), nearshore parametric wave setup future projections (2020–2050), projections of shoreline change of current and future (2005–2100) sea level rise scenarios, satellite-derived shorelines, and vertical land motion rates for the years 2007 to 2020.

Code availability

The code for the coastal change model is available at https://doi.org/10.5066/P95T9188. All other codes are available upon request.

References

69. Tyler, D. et al. *Topobathymetric Model of the Coastal Carolinas, 1851 to 2020* (USGS, 2022); https://doi.org/10.5066/P9MPA8K0
70. Cushing, W. M. et al. *Topobathymetric Model of Coastal Georgia, 1851 to 2020* (USGS, 2022); https://doi.org/10.5066/P9J11VV6
71. Danielson, J. J. et al. Topobathymetric elevation model development using a new methodology—Coastal National Elevation Database. *J. Coast. Res.* **76**, 75–89 (2016).
72. Danielson, J. J., Poppenga, S., Tyler, D. J., Palaseanu-Lovejoy, M. & Gesch, D. B. *Coastal National Elevation Database: Fact Sheet 2018–3037* (USGS, 2018); https://doi.org/10.3133/fs20183037
73. *Coastal National Elevation Database (CoNED) Project - Topobathymetric Digital Elevation Model (TBDEM) for the Atlantic Coast* (USGS, accessed 1 April 2021); https://topotools.cr.usgs.gov/topobathy_viewer/
74. Irwin, J. R., Danielson, J. J. & Robbins, T. J. *Coastal Carolinas Topobathymetric Model: Field Validation Data, 2021* (USGS, 2021); https://doi.org/10.5066/P902W30G
75. *U.S. Coastal Relief Model Vol. 3—Florida and East Gulf of Mexico* (National Geophysical Data Center, accessed 1 April 2021); https://doi.org/10.7289/V5W66HPP
76. *Continuously Updated Digital Elevation Model (CUDEM)—1/9 Arc-Second Resolution Bathymetric-Topographic Tiles* (Cooperative Institute for Research in Environmental Sciences at the University of Colorado, accessed 1 April 2021); https://doi.org/10.25921/ds9v-ky35
77. *USGS One Meter DEM for Florida* (USGS, accessed April 2021); https://rockyweb.usgs.gov/vdelivery/Datasets/Staged/Elevation/1m/Projects/FL_Southeast_B1_2018/
78. Ohenhen, L. O., Shirzaei, M., Ojha, C. & Kirwan, M. L. Hidden vulnerability of US Atlantic coast to sea-level rise due to vertical land motion. *Nat. Commun.* **14**, 2038 (2023).
79. Shirzaei, M. & Bürgmann, R. Topography correlated atmospheric delay correction in radar interferometry using wavelet transforms. *Geophys. Res. Lett.* **39**, L01305 (2012).
80. Shirzaei, M. A wavelet-based multitemporal DInSAR algorithm for monitoring ground surface motion. *IEEE Geosci. Remote Sens. Lett.* **10**, 456–460 (2013).

81. Shirzaei, M., Manga, M. & Zhai, G. Hydraulic properties of injection formations constrained by surface deformation. *Earth Planet. Sci. Lett.* **515**, 125–134 (2019).
82. Lee, J.-C. & Shirzaei, M. Novel algorithms for pair and pixel selection and atmospheric error correction in multitemporal InSAR. *Remote Sens. Environ.* **286**, 113447 (2023).
83. Shirzaei, M. & Walter, T. R. Estimating the effect of satellite orbital error using wavelet based robust regression applied to InSAR deformation data. *IEEE Trans. Geosci. Remote Sens.* **49**, 4600–4605 (2011).
84. O'Neill, A. C. et al. Projected 21st century coastal flooding in the Southern California Bight. Part 1: Development of the third generation CoSMoS model. *J. Mar. Sci. Eng.* **6**, 59 (2018).
85. Barnard, P. L. et al. Development of the Coastal Storm Modeling System (CoSMoS) for predicting the impact of storms on high-energy, active-margin coasts. *Nat. Hazards* **74**, 1095–1125 (2014).
86. Erikson, L. H. et al. Projected 21st century coastal flooding in the Southern California Bight. Part 2: Tools for assessing climate change driven coastal hazards and socio-economic impacts. *J. Mar. Sci. Eng.* **6**, 76 (2018).
87. Leijnse, T. et al. Rapid modeling of compound flooding across broad coastal regions and the necessity to include rainfall-driven processes: a case study of Hurricane Florence. In *Proc. Coastal Sediments 2023* (eds Wang, P. et al.) 2576–2584 (World Scientific, 2023).
88. Parker, K. et al. Relative contributions of water-level components along the US Southeast Atlantic coast from a regional-scale water-level hindcast. *Nat. Hazards* **117**, 2219–2248 (2023).
89. Nederhoff, K. et al. Tropical or extratropical cyclones: what drives the compound flood hazard, impact and risk for the United States Southeast Atlantic coast? *Nat. Hazards* **120**, 8779–8825 (2024).
90. Leijnse, T., van Ormondt, M., Nederhoff, K. & van Dongeren, A. Modeling compound flooding in coastal systems using a computationally efficient reduced-physics solver: including fluvial, pluvial, tidal, wind- and wave-driven processes. *Coast. Eng.* **163**, 103796 (2021).
91. Doran, K. S. et al. *Lidar-Derived Beach Morphology (Dune Crest, Dune Toe, and Shoreline) for U.S. Sandy Coastlines (Ver. 4.0, October 2020)* (USGS, 2017); https://doi.org/10.5066/F7GF0S0Z
92. van Ormondt, M., Leijnse, T., de Goede, R., Nederhoff, K. & van Dongeren, A. A subgrid method for the linear inertial equations of a compound flood model. Preprint at https://doi.org/10.5194/egusphere-2024-1839 (2024).
93. Kahl, D. T., Schubert, J. E., Jong-Levinger, A. & Sanders, B. F. Grid edge classification method to enhance levee resolution in dual-grid flood inundation models. *Adv. Water Resour.* **168**, 104287 (2022).
94. Falgout, J. T., Gordon, J., Williams, B. & Davis, M. J. *USGS Denali Supercomputer* (USGS Advanced Research Computing, accessed 15 July 2024); https://doi.org/10.5066/P9PSW367
95. van Ormondt, M., Nederhoff, K. & van Dongeren, A. Delft Dashboard: a quick setup tool for hydrodynamic models. *J. Hydroinform.* **22**, 510–527 (2020).
96. Muis, S., Verlaan, M., Winsemius, H. C., Aerts, J. C. J. H. & Ward, P. J. A global reanalysis of storm surges and extreme sea levels. *Nat. Commun.* **7**, 11969 (2016).
97. Muis, S. et al. *Global Sea Level Change Time Series from 1950 to 2050 Derived from Reanalysis and High Resolution CMIP6 Climate Projections* (Copernicus Climate Change Service Climate Data Store, 2022); https://doi.org/10.24381/cds.a6d42d60
98. Muis, S. et al. Global projections of storm surges using high-resolution CMIP6 climate models. *Earth's Future* **11**, e2023EF003479 (2023).
99. Stockdon, H. F., Holman, R. A., Howd, P. A. & Sallenger, A. H. Jr. Empirical parameterization of setup, swash and runup. *Coast. Eng.* **53**, 573–588 (2006).
100. Haarsma, R. J. et al. High Resolution Model Intercomparison Project (HighResMIP v1.0) for CMIP6. *Geosci. Model Dev.* **9**, 4185–4208 (2016).
101. Scoccimarro, E., Bellucci, A. & Peano, D. *CMCC CMCC-CM2-VHR4 Model Output Prepared for CMIP6 HighResMIP. Version 20220601* (Earth System Grid Federation, 2017); https://doi.org/10.22033/ESGF/CMIP6.1367
102. Guo, H. et al. *NOAA-GFDL GFDL-CM4 Model Output Prepared for CMIP6 ScenarioMIP SSP585. Version 20190906* (Earth System Grid Federation, 2018); https://doi.org/10.22033/ESGF/CMIP6.9268
103. Roberts, M. J. *MOHC HadGEM3-GC31-HM Model Output Prepared for CMIP6 HighResMIP Highres-future. Version 20191211* (Earth System Grid Federation, 2019); https://doi.org/10.22033/ESGF/CMIP6.5984
104. Roberts, M. J. et al. Projected future changes in tropical cyclones using the CMIP6 HighResMIP Multimodel Ensemble. *Geophys. Res. Lett.* **47**, 2020GL088662 (2020).
105. Nadal-Caraballo, N. C. et al. Coastal hazards system: a probabilistic coastal hazard analysis framework. *J. Coast. Res.* **SI95**, 1211–1216 (2020).
106. Nadal-Caraballo, N. C. et al. *Coastal Hazards System–Louisiana (CHS-LA)* (US Army Engineer Research and Development Center, 2022); https://doi.org/10.21079/11681/45286
107. *Performance Evaluation of the New Orleans and Southeast Louisiana Hurricane Protection System Draft Final Report of the Interagency Performance Evaluation Task Force Volume VIII—Engineering and Operational Risk and Reliability Analysis* (Interagency Performance Evaluation Task Force, 2006).
108. *NOAA National Water Model CONUS Retrospective Dataset* (NOAA, accessed 1 April 2021); https://registry.opendata.aws/nwm-archive
109. Barnard, P. L. et al. *Future Coastal Hazards Along the U.S. North and South Carolina Coasts* (USGS, 2023); https://doi.org/10.5066/P9W91314
110. Barnard, P. L. et al. *Future Coastal Hazards Along the U.S. Southeast Atlantic Coast* (USGS, 2023); https://doi.org/10.5066/P9BQQTCI
111. Niswonger, R. G., Panday, S. & Ibaraki, M. *MODFLOW-NWT, A Newton Formulation for MODFLOW-2005* Techniques and Methods 6-A37 (USGS, 2011); https://doi.org/10.3133/tm6A37
112. *Estimation of Vertical Uncertainties in VDatum* (NOAA, 2018); https://vdatum.noaa.gov/docs/est_uncertainties.html
113. Zell, W. O. & Sanford, W. E. Calibrated simulation of the long-term average surficial groundwater system and derived spatial distributions of its characteristics for the contiguous United States. *Water Resour. Res.* **55**, e2019WR026724 (2020).
114. *USGS Water Data for the Nation* (USGS, accessed 20 December 2021); http://waterdata.usgs.gov/nwis/
115. Haitjema, H. M. & Mitchell-Bruker, S. Are water tables a subdued replica of the topography? *Ground Water* **43**, 050824075421008 (2005).
116. Vitousek, S., Barnard, P. L., Limber, P., Erikson, L. H. & Cole, B. A model integrating longshore and cross-shore processes for predicting long-term shoreline response to climate change. *J. Geophys. Res. Earth Surf.* **122**, 782–806 (2017).
117. Vitousek et al. The application of ensemble wave forcing to quantify uncertainty of shoreline change models. *J. Geophys. Res. Earth Surf.* **126**, e2019JF005506 (2021).
118. Vitousek, S. *CoSMoS-COAST: The Coastal, One-Line, Assimilated, Simulation Tool of the Coastal Storm Modeling System* (USGS, 2023); https://doi.org/10.5066/P95T9188

119. Davidson-Arnott, R. G. Conceptual model of the effects of sea level rise on sandy coasts. *J. Coast. Res.* **21**, 1166–1172 (2005).
120. Wolinsky, M. A. & Murray, A. B. A unifying framework for shoreline migration: 2. Application to wave-dominated coasts. *J. Geophys. Res. Earth Surf.* **114**, F01009 (2009).
121. Davidson-Arnott, R. G. & Bauer, B. O. Controls on the geomorphic response of beach-dune systems to water level rise. *J. Great Lakes Res.* **47**, 1594–1612 (2021).
122. Hersbach, H. et al. *ERA5 Hourly Data on Single Levels from 1940 to Present* (Copernicus Climate Change Service Climate Data Store, accessed 6 August 2020); https://doi.org/10.24381/cds.adbb2d47
123. Vos, K., Harley, M. D., Splinter, K. D., Simmons, J. A. & Turner, I. L. Sub-annual to multi-decadal shoreline variability from publicly available satellite imagery. *Coast. Eng.* **150**, 160–174 (2019).
124. Elko, N. et al. A century of US beach nourishment. *Ocean Coast. Manag.* **199**, 105406 (2021).
125. Jones, J. M., Henry, K., Wood, N. & Jamieson, M. HERA: a dynamic web application for visualizing community exposure to flood hazards based on storm and sea level rise scenarios. *Comput. Geosci.* **109**, 124–133 (2017).
126. *Explore Census Data* (US Census Bureau, accessed 3 March 2023); https://data.census.gov/cedsci/
127. *Homeland Infrastructure Foundation-Level Data* (US Department of Homeland Security, accessed 3 March 2023); https://gii.dhs.gov/hifld/
128. Jones, J. et al. *Community Exposure to Future Coastal Hazards for Florida, USA, Reference Year 2020* (USGS, 2023); https://doi.org/10.5066/P9V3XUNQ
129. Jones, J. et al. *Community Exposure to Future Coastal Hazards for Georgia, USA, Reference Year 2020* (USGS, 2023); https://doi.org/10.5066/P9DCC1HK
130. Jones, J. et al. *Community Exposure to Future Coastal Hazards for U.S. South Carolina, Reference Year 2020* (USGS, 2023); https://doi.org/10.5066/P97XOF91
131. Jones, J. et al. *Community Exposure to Future Coastal Hazards for U.S. North Carolina, Reference Year 2020* (USGS, 2023); https://doi.org/10.5066/P9Q2CCCH
132. Jones, J. et al. *Community Exposure to Future Coastal Hazards for Virginia, USA, Reference Year 2020* (USGS, 2023); https://doi.org/10.5066/P93JG2BN
133. *National Land Cover Database* (Multi-Resolution Land Characteristics Consortium, accessed 3 March 2020); https://www.mrlc.gov/data
134. Erikson, L. H., O'Neill, A., Barnard, P. L., Vitousek, S. & Limber, P. W. Climate change-driven cliff and beach evolution at decadal to centennial time scales. In *Proc. 8th International Conference on Coastal Dynamics 2017* (eds Aagaard, T. et al.) Paper No. 210 (2017).
135. Hauer, M. E. et al. Assessing population exposure to coastal flooding due to sea level rise. *Nat. Commun.* **12**, 6900 (2021).
136. Swain, D. L. et al. Increased flood exposure due to climate change and population growth in the United States. *Earth's Future* **8**, e2020EF00177 (2020).
137. Bates, P. D. et al. Combined modeling of US fluvial, pluvial and coastal flood hazard under current and future climates. *Water Resour. Res.* **57**, e2020WR028673 (2021).

Acknowledgements

Support for this research project was provided by the US Geological Survey's Coastal and Marine Hazards and Resources Program and the Additional Supplemental Appropriations for Disaster Relief Act of 2019 (H.R. 2157) for work focused on North Carolina and South Carolina (P.L.B.). Flood hazard computing was performed at USGS Advanced Research Computing on the Denali Supercomputer[94]. Any use of trade, firm or product names is for descriptive purposes only and does not imply endorsement by the US Government.

Author contributions

P.L.B. conceived the study and led the paper writing. K.M.B. led the groundwater modelling. L.H.E., K.N. and K.A.P. led the flood modelling. A.C.F. and A.C.O. led hazard zone quality assurance and quality control, and internal review. C.M. led the tropical storm modelling. M.S. led the vertical land motion analyses. S.V. led the coastal change modelling. N.J.W. led the socioeconomic analyses. K.M.B., J.J.D., L.H.E., A.C.F., M.K.H., D.J.H., T.W.B.L., C.M., K.N., A.C.O., K.A.P., M.S., P.W.S., J.A.T., S.V. and N.J.W. participated in writing the paper. K.M.B., A.C.E., L.H.E., A.C.F., D.J.H., T.W.B.L., C.M., R.M., N.C.N.-C., K.N., A.C.O., K.A.P., L.O.O., J.A.T., M.v.O., K.V., J.M.J. and J.L.J. participated in developing the analyses.

Competing interests

The authors declare no competing interests.

Additional information

Supplementary information The online version contains supplementary material available at https://doi.org/10.1038/s41558-024-02180-2.

Correspondence and requests for materials should be addressed to Patrick L. Barnard.

Peer review information *Nature Climate Change* thanks Brett Sanders, Shengli Tao and the other, anonymous, reviewer(s) for their contribution to the peer review of this work.